Quantitative investigation of the de Haas-van Alphen effect in the superconducting state

T. J. B. M. Janssen, C. Haworth, S. M. Hayden, P. Meeson, and M. Springford
H. H. Wills Physics Laboratory, University of Bristol, Tyndall Avenue, Bristol, BS8 1TL, United Kingdom

A. Wasserman
Department of Physics, Oregon State University, Corvallis, Oregon, 97331
(Received 19 November 1997)

The de Haas-van Alphen effect in the vortex state of the type-II superconductors 2H-$NbSe_2$ and V_3Si is studied. We discuss the experimental and theoretical considerations pertaining to the observation of such oscillations. Macroscopic pinning of the flux lattice cannot explain the observed attenuation of quantum oscillations in the mixed state. A critical comparison of our measurements with the various microscopic theoretical models describing this phenomenon is made. We show how orientation-dependent de Haas-van Alphen data may be analyzed in a model-dependent way to yield the variation of the superconducting gap over the Fermi surface. [S0163-1829(98)06418-2]

I. INTRODUCTION

The first report of Landau quantum oscillations in the mixed (or vortex) state of a superconductor was made twenty years ago by Graebner and Robbins[1] who observed magnetothermal oscillations in the layered compound 2H-$NbSe_2$. Such observations are very puzzling, as the development of a superconducting energy gap might, at first sight, be thought to eliminate quantum oscillations whose presence has for long been taken as canonical evidence for a Fermi surface. Rather surprisingly, no further experimental work on this phenomenon was published until 1992 when Onuki and co-workers[2] confirmed the observations in the same material but extended the measurements to the lower temperature of 0.3 K. The field of de Haas-van Alphen (dHvA) effect measurements in the vortex state has been widened considerably to include not only 2H-$NbSe_2$,[3–6] but also certain $A15$ compounds, V_3Si (Refs. 7 and 8) and Nb_3Sn,[9] $Ba(K)BiO_3$,[10] $CeRu_2$,[11,12] YNi_2B_2C,[13–16] URu_2Si_2,[17,18] a molecular metal κ-$(BEDT\text{-}TTF)_2Cu(NCS)_2$,[19] and even reported measurements in the high-T_c material $YBa_2Cu_3O_{7-\delta}$.[20–26]

On the basis of this body of experimental evidence, it would seem reasonable to suppose that the dHvA effect is a fundamental property of a type-II superconductor in the vortex state. This realization has already motivated much theoretical work, although the dominant mechanism leading to magnetic quantum oscillations in such an environment has still to be clearly established. Nevertheless, a central theme in each of the theories is the role played by the superconducting energy gap in determining the principal experimental observation: quantum oscillations suffer an additional attenuation in the vortex state, over and above that in the normal state. The possibility then arises of determining the energy gap from the measured attenuation. The dHvA effect probes the anisotropy of quasiparticle states in **k** space so that given an appropriate theoretical foundation, we should anticipate that dHvA effect measurements in the vortex state can yield information on the magnitude and variation of the energy gap over the Fermi surface.

The present study has been undertaken in an attempt to clarify the experimental and theoretical situation. We report below a detailed and quantitative experimental study of the dHvA effect in the two superconductors 2H-$NbSe_2$ and V_3Si. Being available as single crystals of high quality, each permits the dHvA effect to be measured, with precision, over a wide field range.

This paper is organized as follows. Section II gives an introduction to the de Haas-van Alphen effect in a normal metal. In Sec. III some of the relevant theoretical models describing the dHvA effect in the vortex state are reviewed. In Sec. IV some important considerations concerning the experimental observation of the dHvA effect in the vortex state are discussed. In Sec. V the experimental results and analysis of the quantum oscillations in the vortex state of $NbSe_2$ and V_3Si are presented and discussed. A discussion of our results is given in Sec. VI. Finally, in Sec. VII we briefly summarize our results.

II. THE de HAAS-van ALPHEN EFFECT IN A NORMAL METAL

The dHvA effect is an oscillatory contribution to the magnetization $\tilde{\mathbf{M}}$ of a metal, which is periodic in the inverse applied magnetic field $\mathbf{B}_0^{-1}$, where $\mathbf{B}_0=\mu_0\mathbf{H}$. In the normal state, dHvA oscillations are conventionally interpreted using the semiclassical Lifshitz-Kosevich (LK) theory for a collection of weakly interacting quasiparticles.[27] The frequency and amplitude of the oscillations provide information about the low-energy quasiparticles. Each extremal cross-sectional area A of the Fermi surface in the plane normal to the applied field $\mathbf{B}_0$ gives an infinite series of oscillatory components to $\tilde{\mathbf{M}}_{\mathrm{LK}}$ with fundamental frequency $F=(\hbar/2\pi e)A$ given by

$$\tilde{M}_{\mathrm{LK}} \propto \sum_{r=1}^{\infty} \alpha(B_0,T,r)\sin\left[2\pi r\left(\frac{F}{B_0}-\frac{1}{2}\right)\pm\frac{\pi}{4}\right], \qquad (1)$$

where

$$\alpha(B_0,T,r)=B_0^{-1/2}\frac{T}{\sinh(2\pi^2 r k_B T m^\star/e\hbar B_0)} \times\cos\left(\frac{r\pi g m_b\Gamma}{2m_e}\right)\exp\left(-\frac{r\pi m_b}{eB_0\tau_0}\right)R_s, \quad (2)$$

$$m_b=\frac{\hbar}{2\pi}\oint_{\text{orbit}}\frac{dk}{v_F(\mathbf{k})}, \quad (3)$$

and $R_s=1$ in the normal metallic state. The exponential factor (Dingle factor) in Eq. (2) accounts for the scattering due to static defects and impurities, τ_0^{-1} being the quasiparticle scattering rate. Alternatively, one can express the damping as a Landau level broadening $\hbar/2\tau_0$ or Dingle temperature $\hbar/2\tau_0=\pi k_B T_D$. Γ is the many-body exchange (or Stoner) enhancement of the Pauli susceptibility.[28]

Three ''electron masses'' appear in Eq. (2), the mass of the electron is denoted by m_e. The difference between these masses has been discussed in the literature,[28–31] we summarize these below. We denote the ''band mass'' computed from Eq. (3) by m_b. In this equation the Fermi velocity $v_F=(1/\hbar)(dE/dk)$ is calculated from a quasiparticle band structure as envisaged by Hohenberg, Kohn, and Sham.[32,33] We note that m_b is not directly measured by de Haas-van Alphen experiments (see below). The ''renormalized mass'' $m^\star$ occurs in the sinh factor in Eq. (2) and *can* be measured directly from the temperature dependence of the amplitude of the dHvA oscillations. Appropriately averaging this mass over all sheets of the Fermi surface would yield the electron mass determined from specific heat measurements. The renormalized mass $m^\star$ differs from m_b in that it includes the effects of interactions of the electrons with excitations such as phonons, magnons, and other magnetic excitations. The presence of these low-frequency degrees of freedom can lead to a large enhancement of $m^\star$ over m_b. It has been shown theoretically that the factor m_b/τ_0 in the exponential or Dingle factor of Eq. (2) is unaffected by the electron-phonon interaction[29] and is also believed to be unaffected by other electron interactions.[28]

III. THE de HAAS-van ALPHEN EFFECT IN THE VORTEX STATE

A. Field inhomogeneity in the vortex state

The observation of the dHvA effect requires stringent conditions on the *macroscopic* homogeneity of the magnetic field $B(\mathbf{r})$ within the sample. Field inhomogeneities result in a loss of phase coherence between dHvA oscillations from different parts of the sample and hence a suppression of the overall amplitude. The formation of the flux line lattice (FLL) on entering the mixed state introduces a somewhat different complication: a *microscopic* field variation, that is on a length scale less than the cyclotron orbit radius r_c. It has been suggested that the suppression of the dHvA oscillations can be explained by ''phase smearing'' as a result of the inhomogeneous magnetic field distribution within the superconducting vortex state.[2,7,11] In order to determine whether the field inhomogeneity due to the FLL itself needs to be included in our consideration of the dHvA effect in the superconducting state, a numerical estimate of this effect was performed for an ideal type-II superconductor with a hexagonal FLL.

We consider the highest occupied Landau level. Within the semiclassical approximation, the flux threading the corresponding cyclotron orbit in real space is quantized:

$$\phi=\int\mathbf{B}(\mathbf{r})\cdot\mathbf{dS}=(n+\gamma)\frac{2\pi\hbar}{e}. \quad (4)$$

The inhomogeneous field implies that for a given Landau index n the orbit size will vary according to the location of its center in the FLL. To our knowledge, there are no direct measurements by neutron scattering or muon spin resonance of the magnetic field distribution for large κ materials at the fields ($\approx$10 T) used in the present experiments. There are, however, a number of theoretical treatments, which have been experimentally confirmed at lower fields,[34,35] which give an estimate of the magnetic field distribution within the Ginzburg-Landau formalism. The magnetic field within a clean superconductor close to B_{c2} can be described as[35]

$$B(\mathbf{r})=\langle B(\mathbf{r})\rangle+\mu_0|M|\sum_{\mathbf{K}\neq\mathbf{0}}b_{\mathbf{K}}\cos\mathbf{K}\cdot\mathbf{r}, \quad (5)$$

where $\langle B(\mathbf{r})\rangle$ is the spatially averaged induction and $\mu_0 M=B_0-\langle B(\mathbf{r})\rangle$ is the magnetization.

For a hexagonal FLL with lattice parameter a, the reciprocal lattice vector $\mathbf{K}=\mathbf{K}_{mn}=(2\pi/a)[\hat{\mathbf{x}}m+\hat{\mathbf{y}}(2n+m)/\sqrt{3}]$ (the applied field B_0 parallel to the z axis). At low temperatures ($T\ll T_c$) the Fourier coefficients $b_{\mathbf{K}}$ are approximately[34] given by $b_{\mathbf{K}}\approx(-1)^\nu(3^{3/4}/2\pi)/\nu^{3/2}$, where $\nu=m^2+mn+n^2$. In the simulation we only use the Fourier components with $\nu=1$. The magnetization is given by[35]

$$M=\frac{1}{\mu_0}\frac{B_{c2}-B_0}{(2\kappa^2-1)\beta_A}, \quad (6)$$

where κ is the Ginzburg-Landau (GL) parameter and $\beta_A=1.1596$ for the hexagonal FLL. Strictly speaking, this equation only applies in the dirty limit close to T_c. In the clean limit $l\gg\xi$, as is the case for the materials studied in this work, κ diverges for $T\to0$ and $B_0\approx B_{c2}$ which implies that M vanishes.[36,37] Therefore, Eq. (6) represents an upper bound for the magnetization.

To calculate the distribution of areas of orbits linking the same magnetic flux, we first sample cyclotron orbits of fixed area with random centers in the FLL unit cell [see Fig. 1(a)]. The set of randomly sampled orbits has fluxes $\{\phi_i\}$ and a typical distribution $P(\phi)$ shown in Fig. 1(b) calculated for the parameters of V_3Si. (V_3Si has a lower κ value than $NbSe_2$ and hence the effect of the field inhomogeneity will be stronger.) The field dependence of the standard deviation of the distribution $\delta\phi$ is shown in Fig. 2(a). The variation of $\delta\phi$ as a function of the applied magnetic field shows sharp minima which are found to be periodic in $1/\sqrt{B}$. This behavior can be simply understood as a ''geometrical resonance'' of the cyclotron orbit size r_c with the FLL lattice parameter a. The minima in $\delta\phi$ occur such that $r_c\propto na$ where n is an integer.

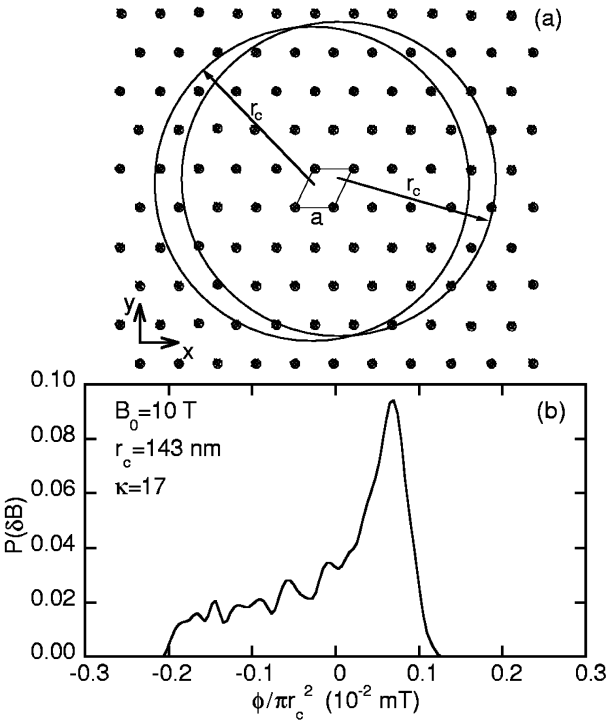

FIG. 1. (a) Schematic of a triangular flux-line lattice with lattice parameter a and unit cell $(a\hat{\mathbf{x}},2a/\sqrt{3}\hat{\mathbf{y}})$ with the applied field parallel to the z axis. Two cyclotron orbits are shown with different centers within the FLL unit cell. Note that the cyclotron radius in this picture is drawn 5 times smaller than the actual size. In the simulation we calculate the flux through typically 1000 orbits with random centers in the unit cell, producing a probability distribution such as shown in (b). (b) $P(\phi)$ versus ϕ, plotted as the deviation from the average flux, calculated for the parameters of V_3Si.

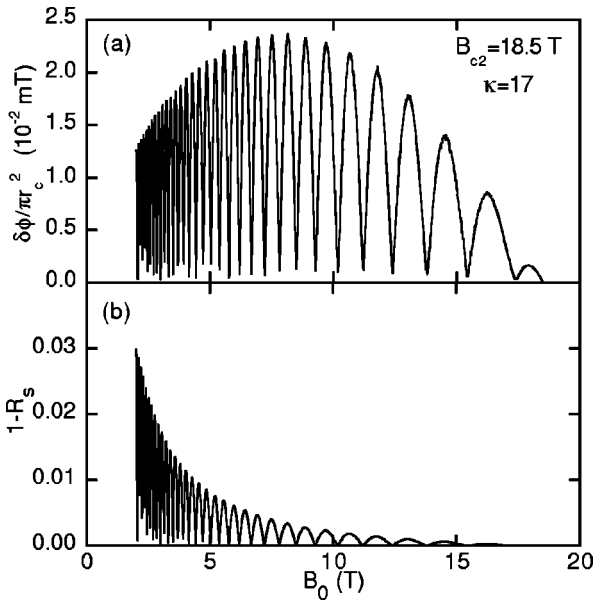

FIG. 2. (a) Variation of the standard deviation, $\delta\phi$, of the calculated probability distributions, such as displayed in Fig. 1(b), as a function of the applied magnetic field B_0. The oscillations are periodic in $1/\sqrt{B_0}\propto na$. (b) Damping expressed as $1-R_s$ resulting from the field inhomogeneity, versus magnetic field.

To obtain the corresponding distribution of areas of orbits linking the *same* flux, we note that in the limit $|B(\mathbf{r})-\langle B(\mathbf{r})\rangle|\ll B_0$ such orbits can be obtained by increasing (or decreasing) the area by $(\phi_i-\langle\phi_i\rangle)/B_0$. The standard deviation of the distribution of areas is $\delta\phi/B_0$ and the corresponding spread of reciprocal space areas is $(eB_0/\hbar)^2\delta\phi/B_0$. Using the fact that $F=(\hbar/2\pi e)A$, the spread in orbit sizes gives rise to an apparent spread in dHvA frequencies[27] $\delta F=(\hbar/2\pi e)(eB_0/\hbar)^2\delta\phi/B_0$. This results in an additional field-dependent factor in the amplitude

$$R_s=\exp\left(-\frac{2\pi\delta F}{B_0}\right). \tag{7}$$

The magnitude of $1-R_s$ is about two orders of magnitude smaller than the observed values of $1-R_s$ reported in Sec. V. We therefore conclude that the direct effect of the microscopic field inhomogeneity due to the vortex lattice has a negligible effect on the amplitude of the dHvA oscillations under the present conditions.

B. Microscopic theories

A number of theoretical models have been proposed to explain the persistence of the dHvA effect below B_{c2} in a type-II superconductor. We begin with a brief discussion in order to highlight their distinguishing features. In particular, we identify the form of the magnetic field dependence of the dHvA effect. We note that there are also models applicable only to two-dimensional (2D) systems[38–41] which are not applicable to the materials considered in the present investigation. Although $NbSe_2$ is a layered compound, the Fermi surface feature studied here is three dimensional[3] in the sense that the variation of the cross-sectional area of the Fermi surface perpendicular to the applied field is much greater than the difference in area of consecutive Landau orbits $2\pi eB_0/\hbar$.

A common feature of all the theoretical models is the suppression of the dHvA oscillations with respect to the standard LK formula [Eq. (1)]. It is convenient to describe this suppression through the factor R_s in Eq. (1). In describing the experimental data, it is convenient to define a ''scattering rate'' τ_s^{-1} due to the superconductivity through the relation

$$R_s=\exp\left(-\frac{\pi r m_b}{eB_0\tau_s}\right). \tag{8}$$

Several of the microscopic models can be couched in this form. The microscopic theories which consider explicitly[28,42,43] which mass occurs in Eq. (8) use the band mass m_b rather than the effective mass $m^\star$.

The damping of quantum oscillations in the mixed state is presumed to include the influence of impurities and static defects, as observed in the normal state, in addition to that arising from superconducting order. Hence, parametrizing the damping due to superconducting order by $\tau_s^{-1}(B_0,T)$, we may write for the total scattering rate $\langle\tau^{-1}\rangle=\langle\tau_0^{-1}\rangle+\langle\tau_s^{-1}\rangle$, in which $\langle\cdots\rangle$ designates an orbitally averaged value. This additive relation, or ''orbital Mattheissen rule'' will break down if τ_0^{-1} is influenced by the superconductivity or if the anisotropies of $\tau_0^{-1}(\mathbf{k})$ and $\tau_s^{-1}(\mathbf{k})$ differ. We

note that the microscopic theory of Dukan and Tešanović (discussed below) explicitly *does not* assume the orbital Mattheissen rule.

The superconducting gap Δ enters all of the models discussed below. In the absence of measurements of the field-dependent superconductor gap, we use the equation

$$\Delta(B_0)=\Delta(0)\sqrt{1-\frac{B_0}{B_{c2}}} \tag{9}$$

to describe the field-dependence of the superconducting gap. This form has considerable theoretical justification.[35]

1. Theories of Maki, Stephen, and Wasserman and Springford (MSWS)

The approach of Maki[44] is based on semiclassical approximations for the electron Green function in the mixed state. The approximation first introduced by Brandt *et al.*[45] was to retain only the spatially averaged value of Δ^2. The existence of a gapless excitation spectrum is also a feature of Brandt's approach.[45] Whereas excitations with **k** parallel to **B** have the familiar BCS form, those in planes perpendicular to **B** are gapless. Because it is precisely the latter that are probed in a dHvA experiment, the physical origin of quantum oscillations in the superconducting state is due to this gaplessness. Maki finds that the dHvA oscillations have an extra damping [Eq. (8)] in the superconducting state where τ_s^{-1} is now given by

$$\hbar\tau_s^{-1}=\frac{2\sqrt{\pi}\Delta^2(B_0)\Lambda}{v_{\mathrm{F}}} \tag{10}$$

or

$$R_s=\exp\left[-\pi^{3/2}\left(\frac{\Delta m_b}{\hbar eB_0}\right)^2\left(\frac{B_0}{F}\right)^{1/2}\right], \tag{11}$$

where $\Lambda=(2\hbar eB_0)^{-1/2}$, v_{F} is the Fermi velocity. The quantities on the right hand side of Eq. (10) may vary around the orbit, e.g., in $NbSe_2$, the Fermi velocity is anisotropic. In this case we interpret Eq. (10) to be orbitally averaged and use $\langle 1/v_{\mathrm{F}}\rangle=m_b/\sqrt{2\hbar eF}$. Stephen[46,47] obtained Maki's result by solving the Bogoliubov–de Gennes (BdG) equations for magnetic fields close to B_{c2} (small Δ) but his result, a quantized energy spectrum with level spacing $\hbar\omega_c$, differs from that of Dukan and Tesanovic.[42]

Wasserman and Springford[43] incorporated Brandt's self-energy in a general field-theoretic expression for the dHvA effect in an interacting system[28] in which the real and imaginary parts of the electron self-energy evaluated on the *imaginary energy* axis renormalize the frequency and amplitude terms in the original LK formula whilst leaving its general structure unaltered. The real part of the self-energy vanishes corresponding to no change in the dHvA frequency (Stephen's[47] approach predicts a small energy shift). The imaginary part, however, is finite and contributes an extra damping term identical to Eq. (10). In the above models, the damping is determined by the *spatially averaged* value of Δ^2, a result which underlines its insensitivity to the degree of order in the vortex lattice. The inclusion of higher order terms representing Fourier components of the 2D periodic order parameter associated with the ordered vortex lattice, is straightforward, but was found by Wasserman and Springford not to add significantly to the result expressed in Eq. (10).

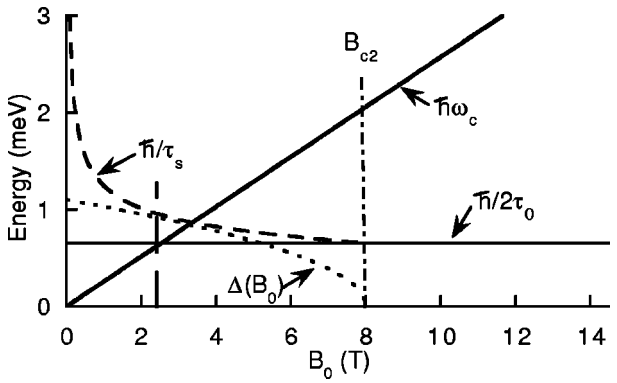

FIG. 3. Schematic diagram showing the relevant energies as a function of magnetic field calculated for the parameters of $NbSe_2$. The angle between magnetic field and c axis is 68.6°. The solid line is the cyclotron energy $\hbar\omega_c$, the dotted line is the superconducting energy gap calculated using the BCS relation with $\Delta(0)$ taken to be the BCS value of 1.1 meV. The long dashed line is the field-dependent damping due to the vortex state calculated using Eq. (10). The horizontal solid line represents the field independent Landau level broadening due to impurity scattering.

In Fig. 3 we illustrate the various contributions in this model for the material $NbSe_2$ (details for this material are given below). $\hbar/2\tau_0$ represents the Landau-level broadening due to impurity scattering and $\hbar\omega_c$ is the Landau-level spacing. Ignoring the vortex state, the classical limit for observing the quantum oscillations is given by the condition $\hbar/2\tau_0\approx\hbar\omega_c$ (marked by the dashed vertical line). When the vortex state is included, a superconducting gap develops below B_{c2}, which leads to an additional broadening of the Landau-levels given by Eq. (10). In this picture τ_0 is taken to be a constant as a function of magnetic field, independent of whether a vortex state is present or not. This assumption may not be true, but seems to be supported by the field theoretical model of Wasserman and Springford. Figure 3 illustrates the increased magnetic field dependent damping in the vortex state as the gap parameter develops.

2. Theory of Miyake (MMG)

Miyake[48] considered the extreme type-II limit $\kappa\gg 1$ and neglected the spatial variation of the superconducting gap Δ. BCS-quasiparticle states are then quantized using the semiclassical Bohr-Sommerfeld rule. An expression for the oscillatory magnetization can then be obtained following the usual Lifshitz-Kosevich method. The result of such a calculation yields an additional factor

$$R_s=\alpha K_1(\alpha) \tag{12}$$

in the superconducting state, where $\alpha=2\pi r\Delta m_b/\hbar eB_0$. $K_1(z)$ is the Bessel function of imaginary argument. In this theory, the contributions of the normal core regions are neglected. The damping in the superconducting state results from replacing the sharp step in the Fermi-Dirac occupation function with BCS quasiparticle energies and occupation functions. Miller and Györffy[49] have derived the same results starting from the BdG equation (see below). For the

case of a simple BCS superconductor, where the gap parameter is isotropic, this model predicts a large attenuation of the quantum oscillations in the vortex state. If, however, the gap vanishes at some point(s) or line(s) on the Fermi surface, the size of R_s becomes of order unity (small damping) when the cyclotron orbit in **k** space passes through such zeros even if the gap parameter on other parts of the cyclotron orbit is sizable.

3. Theory of Dukan and Tešanović (DT)

This approach[42] rests upon the observation that, in the quantum limit ($\hbar\omega_c \gg \Delta$) where the Landau levels can be treated explicitly, $\Delta(\mathbf{r})$, the spatial dependent order parameter, goes to zero at sites corresponding to the positions of the vortex cores. The excitation spectrum, calculated by analytically solving the BdG equations, is found to be ''gapless'' at a related set of points in the magnetic Brillouin zone of the flux lattice. Furthermore, with some modification, this behavior persists to relatively low fields, far below B_{c2}.[50] The physical origin of the dHvA effect in the vortex state is traced to this particular feature of the excitation spectrum. The oscillatory part of the thermodynamic potential in the superconducting state is then calculated in the presence of this gapless spectrum. Oscillatory contributions to the potential are divided into two components, one from the gapless region and a second but negligible contribution from the remainder of the (gapped) Fermi surface. The gapless region G has an area attributed to it that is essentially the sum of the normal areas around the nodes. In reciprocal space G has a radius q_c given by

$$q_c = C\ \max\left(\frac{T}{\Delta}, \frac{\Gamma}{\Delta}\right), \tag{13}$$

where C is a constant of order unity, Γ is the imaginary part of the electron self-energy related to the total effective scattering rate τ_{tot}^{-1} by $\Gamma = \hbar/2\tau_{\mathrm{tot}}$, and Δ is defined as the amplitude of the order parameter. A self-consistent calculation of Γ when $\Delta > 2\Gamma_0$ yields

$$\Gamma(B_0) = \sqrt{\frac{\Gamma_0 \Delta(B_0)}{2}}, \tag{14}$$

where Γ_0 is the value in the normal state and the magnetic field dependence of Δ is taken into account via the Ginzburg-Landau equation

$$\Delta(B_0) = \Delta(0)\left(1 - \frac{B_0}{B_{c2}}\right)^{1/2}. \tag{15}$$

This leads to the amplitude of the fundamental harmonic of the dHvA effect in a superconductor containing an additional term to that in the normal state,

$$R_s = 2\left[C\ \max\left(\frac{T}{\Delta}, \frac{\Gamma}{\Delta}\right)\right]^2 \exp\left(\frac{-\pi m_b}{eB_0\tau_{\mathrm{tot}}}\right), \tag{16}$$

with $\hbar\tau_{\mathrm{tot}}^{-1} = 2\Gamma(B_0)$ for $\Delta > 2\Gamma_0$ and $\hbar\tau_{\mathrm{tot}}^{-1} = 2\Gamma_0 = \hbar\tau_0^{-1}$ for $\Delta < 2\Gamma_0$.

4. Theory of Miller and Györffy (MG)

In this approach[49] the BdG equations corresponding to a simple tight binding model in a magnetic field are solved using a real-space recursion method, to give a self-consistent microscopic solution for the Abrikosov flux lattice. A key result is the appearance of a discrete Landau-level-like structure in the density of states spectrum, even in the presence of a large order parameter. The ground state is visualized as being formed from Cooper pairs of electrons which occupy discrete ''Landau levels.'' With changing magnetic field, the levels adjust in a manner not dissimilar to the case of a normal metal leading to quantum oscillations in the thermodynamic potential with the same period. The origin of the dHvA effect in the vortex state is identified with this underlying quantization of the superconducting ground state energy. Although the frequency of quantum oscillations is unchanged in this model from its value in the normal state, the amplitude is diminished according to Eq. (12) essentially because the thermodynamic potential includes the variation of particle occupation number $|u_k|^2$ which changes over an energy region on the scale of Δ, the magnitude of the order parameter.

5. Theory of Norman, MacDonald, and Akera (NMA)

NMA (Ref. 51) also seek a solution of the mean field gap BdG equations in the vortex state in the presence of Landau quantization of the energy levels, although their approach is based on a different formalism. Again, gapless branches of the excitation spectrum are a feature of their solution as in the previous model. The magnetic field is assumed uniform throughout the superconductor and the free energy and hence magnetization calculated for a representative model of a weak-coupling superconductor. Although direct comparison of these results with experiments on specific materials is difficult, estimates of the additional damping due to the presence of a superconducting order parameter can be made by introducing an amplitude reduction factor for the fundamental dHvA harmonic as in Eq. (8). Near B_{c2} and neglecting off-diagonal pairing, the superconducting relaxation rate τ_s^{-1} is found to be,

$$\hbar\tau_s^{-1} \approx 0.6 n^{-1/4} k_{\mathrm{B}} T_c \left(1 - \frac{B_0}{B_{c2}}\right)^{1/2}, \tag{17}$$

which incorporates the Ginzburg-Landau form of the field dependence of T_c. The presence of $n^{-1/4}$, in which n is the Landau level index, means that small pieces of Fermi surface suffer stronger damping than larger ones. Using a theoretical model to infer the full damping when inter-Landau level (off-diagonal) pairing is included, they find that the relaxation rate is enhanced by approximately 3.5, so that Eq. (17) becomes

$$\hbar\tau_s^{-1} \approx n^{-1/4}\Delta'(B_0), \tag{18}$$

in which $\Delta'(B_0, T)$, is directly related to the energy gap, but by an unspecified numerical constant.

In a later report Norman and McDonald[52] studied the magnetic quantum oscillations in the vortex state in greater detail and noted that the actual behavior is more complicated. They argue that a crossover regime exists from linear

to quadratic behavior in the order parameter when the quantity $F_0/n^{1/4}$ falls below $2\pi k_B T$, where F_0 is defined in Ref. 51 as the vortex lattice analogue of the BCS gap. This implies that at higher temperatures the relaxation rate takes the form

$$\hbar\tau_s^{-1} \approx n^{-1/2}\Delta'^2(B_0). \tag{19}$$

In the crossover regime both terms should be present.[53]

6. Theory of Maniv, Rom, Vagner, and Wyder (MRVW)

MRVW (Refs. 38–41) start with a Gorkov-Ginzburg-Landau like expansion of the free energy in the superconducting state to forth order in the superconducting order parameter. For a two-dimensional (2D) superconductor, they find a new contribution to the dHVA oscillations which is in antiphase with normal state oscillatory magnetization. The total oscillatory magnetization corresponds to

$$R_s = 1 - \pi^{3/2}\left(\frac{\Delta m_b}{\hbar e B_0}\right)^2\left(\frac{B_0}{F}\right)^{1/2}. \tag{20}$$

In the limit of small Δ^2 this is the same as the MSWS form, however, the MRVW theory is strictly only applicable in the 2D limit.

IV. EXPERIMENTAL CONSIDERATIONS

The experiments described in this work were performed in a cryomagnetic system incorporating a top-loading dilution refrigerator with a base temperature of 17 mK and a superconducting solenoid providing a field of 13.6 T at 4.2 K. The field modulation method of detection was used at modulation frequencies in the range 1–20 Hz. Some of the experiments were performed in a 60 T pulsed magnet system at temperatures down to 1.2 K. The single crystal samples used have each been described in earlier work.[3,8] Details of the properties and bandstructures of these materials can be found in these articles and references therein. Before we present the experimental results in the next section we discuss some of the experimental issues pertaining to the observation of the dHvA effect in the vortex state of a superconductor.

A number of techniques are used for the detection of quantum oscillations in metals; these include field modulation, pulsed techniques, and torque magnetometry. Magnetothermal oscillations were initially detected by a field modulation technique, while dHvA (magnetization) oscillations have been detected both by field modulation and pulsed field methods. Most of the measurements presented in this paper were made using a field modulation technique in which an oscillatory field $b(t) = b_0\cos(\omega t)$ is superimposed parallel to a ''quasistatic'' field B_0 which increases (or decreases) slowly ($\dot{B}_0 \ll b_0\omega$) at a constant rate. Below we consider what effect the formation of the vortex state has on measurements performed in this way.

A. dHvA measurements in the presence of pinning

In real superconductors flux lines are pinned by inhomogeneities in the material, e.g., dislocations, vacancies, and grain boundaries. The pinning of flux lines has been discussed extensively.[54] Pinning has a number of consequences concerning the present measurements. (1) The magnetization $M(B)$ and the field distribution within the superconductor $B(\mathbf{r})$ are history dependent and M displays a hysteresis loop when the applied field is cycled. (2) The dHvA amplitude will be decreased because of the variation of the magnetic field over the sample (''phase smearing'') and the partial penetration of the modulation field into the sample. In the following section we use a Bean model analysis to estimate the effect of pinning on our dHvA measurements.

1. ac magnetic response in the mixed state

A quantitative picture of the effect of pinning is afforded by the Bean model.[35,55] In its original version, this model assumes a B-independent critical current density J_c. We consider the response of a flat superconducting slab to a low frequency ac field superimposed on a constant field, $B_a(t) = B_0 + b_0\cos(\omega t)$. The applied field B_a is assumed to be along the z direction and the thin dimension of the slab is along x. The Maxwell equation $\mathrm{curl}(\mathbf{B}) = \mu_0\mathbf{J}$ then yields $-\partial B_z/\partial x = \mu_0 J_y$. If the applied field is increased from zero to $B_a = B_0 + b_0$, the resulting field distributions inside the superconductor are shown in Fig. 4(a), where $B^\star = \frac{1}{2}\mu_0 J_c a$. Here we have considered three separate regimes depending on the relative magnitude of b_0 and $B^\star$. Upon decreasing the applied field to $B_0 - b_0$ the resulting field profiles are shown in Fig. 4(b). The average fields $\langle B\rangle = \int B(x)\,dx/\int dx$ in each case can easily be calculated; these are

$$\left.\begin{aligned}\langle B\rangle_\uparrow &= B_0 + b_0 - B^\star/2\\ \langle B\rangle_\downarrow &= B_0 + b_0 - B^\star/2 - b_0^2/B^\star\end{aligned}\right\} \text{for } b_0 < B^*,$$

$$\left.\begin{aligned}\langle B\rangle_\uparrow &= B_0 + b_0 - B^\star/2\\ \langle B\rangle_\downarrow &= B_0 - b_0 + B^\star/2\end{aligned}\right\} \text{for } b_0 > B^\star, \tag{21}$$

$$\left.\begin{aligned}\langle B\rangle_\uparrow &\approx B_0 + b_0\\ \langle B\rangle_\downarrow &\approx B_0 - b_0\end{aligned}\right\} \text{for } b_0 \gg B^\star.$$

Note that for $b_0 \gg B^\star$ the effect of pinning is minimal and the resulting field distribution homogeneous.

The hysteresis loops obtained in each case are shown in Fig. 4(c), from which it is observed that the modulation field *inside* the superconductor depends critically on the relative magnitudes of b_0 and $B^\star$, and therefore on the magnetization (or critical current J_c) and the geometry of the sample. For a real superconductor the critical current J_c is not B independent as assumed in the Bean model and consequently the magnitude of the hysteresis will change as a function of magnetic field. This will result in an average modulation field inside the superconductor which is B dependent and affects the measured amplitude of the dHvA oscillations.

We have measured the hysteresis loops generated by the modulation field for the $NbSe_2$ sample used in the dHvA experiments. Figure 5 shows a collection of hysteresis loops measured at several different values of the constant main magnetic field B_0. In order to intensify the effect of pinning the modulation amplitude was set at $b_0 = 2$ mT which is about 25 times smaller than the modulation amplitude used in the dHvA experiments. The hysteresis loops were mea-

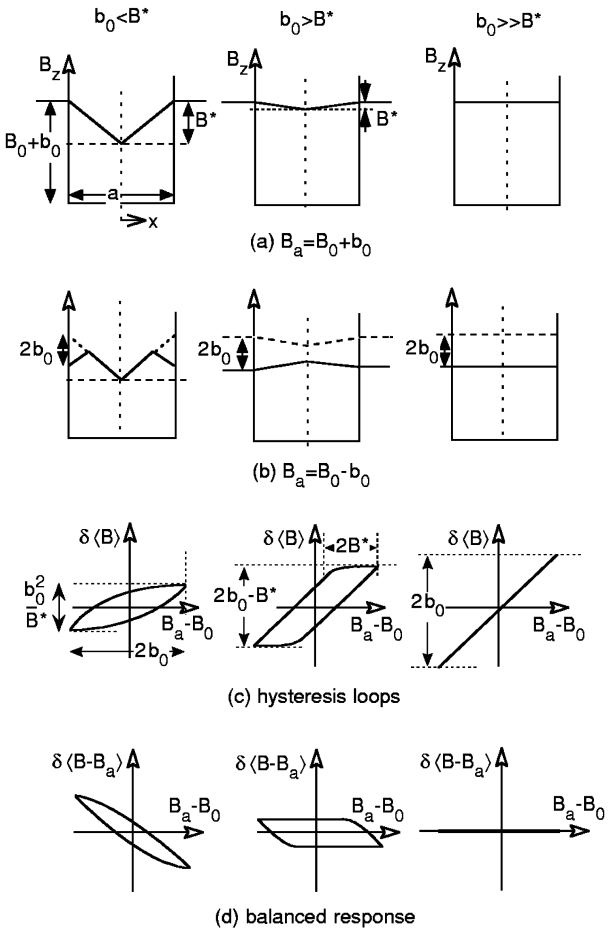

FIG. 4. Field profiles for a flat superconducting slab according to the Bean model. The magnetic field is increased from zero to $B_a = B_0 + b_0$ giving rise to the profiles shown in (a) according to the relative magnitudes of b_0 and $B^\star$. Upon decreasing the field by $2b_0$ (the range of the modulation field), the profiles in (b) are obtained. (c) Calculated hysteresis loops produced by the modulating magnetic field $b(t) = B_a(t) - B_0$. The vertical axis is $\delta\langle B\rangle(t) = \langle B\rangle(t) - B_0$ which is proportional to the magnetization. Finally, the balanced response (a second coil is used to subtract the field in the absence of sample) is shown in (d).

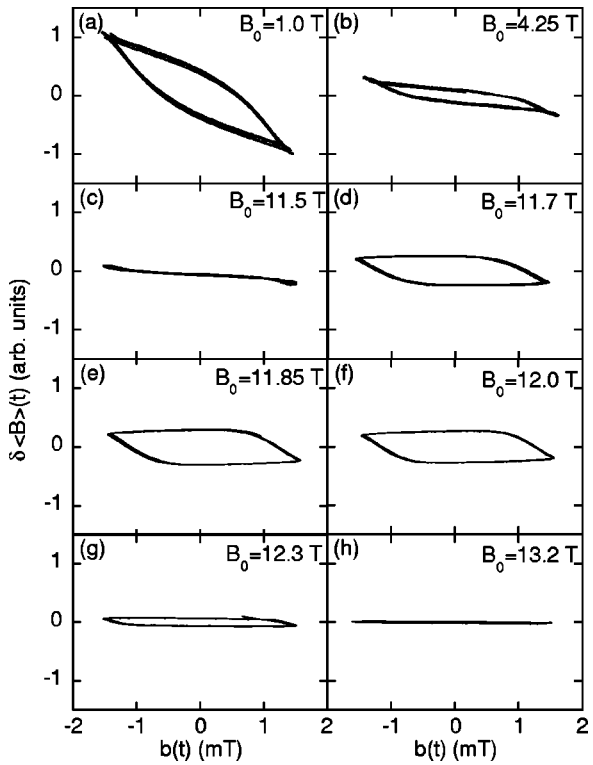

FIG. 5. Measured hysteresis loops at several different magnetic fields for the $NbSe_2$ sample. The x axis is obtained by time integrating the signal from one half of the balanced pick-up coil and is proportional to the modulation field $b(t) = b_0 \cos\omega t$ with $b_0 \approx 2$ mT and $f = 4.8$ Hz. (In the dHvA experiments $b_0 \approx 50$ mT.) The y axis is obtained by time integrating the signal from the total balanced pick-up coil and is proportional to $\delta\langle B\rangle(t)$ (i.e., the magnetization). The pick-up coils were electronically balanced, to give zero response, in the normal metallic state at 13.5 T just above B_{c2}.

sured with the pick-up coils balanced to give zero response in the normal state just above B_{c2}, i.e., the normal state response $M(B)$ is subtracted. The response in the normal metallic state is similar to the case depicted in Fig. 4(c) for $b_0 \gg B^\star$. Therefore, in order to compare the measured hysteresis loops in Fig. 5 with the calculated loops in Fig. 4, we must subtract this normal state response from the responses in Fig. 4(c). The height of the hysteresis loops in Fig. 4(d) will then be given by $2b_0 - b_0^2/B^\star$ for $b_0 < B^\star$, $B^\star$ for $b_0 > B^\star$, and zero for $b_0 \gg B^\star$.

The height of the hysteresis loops can also be obtained by measuring the ac response at the fundamental of the modulation frequency, which is shown in Fig. 6, giving a qualitative measure of $B^\star$ as a function of magnetic field. The signal also contains a contribution of the background susceptibility and is thus not directly proportional to $B^\star$ and J_c. For illustration the magnetic field dependence of J_c is shown schematically in the inset of Fig. 6.

Figure 6 suggests that the response of the flux lattice to a modulation field can be split into three different regimes. The superconducting transition occurs at a field of ≈ 13.3 T, as indicated by the onset of the so-called ''peak effect'' [region (I) in Fig. 6]. The peak effect (which stretches from ≈ 13.3 down to ≈ 11.5 T) is due to pinning of the vortices in a field regime where the flux lattice is soft and thus able to distort easily.[56,57] From a comparison of the measured hysteresis loops in Fig. 5 in the peak effect region with the calculated loops in Fig. 4(d), we can conclude that for this regime the response is similar to the situation depicted for $b_0 > B^\star$. For fields just below the peak effect region the elastic constants of the flux lattice decrease (as the vortex lines become more widely spaced and interactions reduce) and the average effect of the pinning centers is reduced [region (II) in Fig. 6]. This region stretches from ≈ 11.5 down to ≈ 4 T, which corresponds to the case for $b_0 \ll B^\star$ in Fig. 4(d). In the low field limit the number of vortices is small and so the intervortex spacing is necessarily large [region (III) in Fig. 6]. This means that the elastic constants of the flux lattice are small and the flux lattice can be easily distorted near pinning sites. From comparing the measured hysteresis loop at 1 T, with the calculated loop shown in Fig. 4(d), we conclude that for the low field regime $b_0 < B^\star$.

2. Quantitative estimation of the attenuation due to pinning

In the present study, we were unable to record dHvA oscillations in the peak effect region just below B_{c2} due to

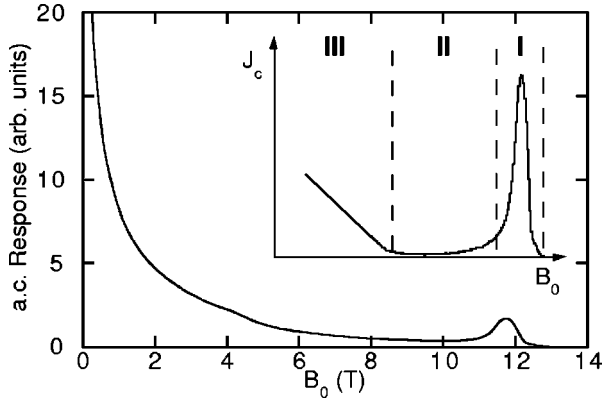

FIG. 6. Measured ac response (i.e., the signal at the fundamental of the modulation frequency) as a function of magnetic field for $NbSe_2$ at a temperature of 20 mK with the magnetic field perpendicular to the crystal c axis. The normal-state ac response at 13.5 T has been subtracted. The signal amplitude of the ac response corresponds to the height of the hysteresis loop as displayed in Fig. 4. The inset shows a schematic of the critical current versus magnetic field. The three indicated regimes correspond to (I) peak effect region where pinning is strong, (II) region where pinning is weak, and (III) region where pinning increases again.

the rapid variation of the non-oscillatory component of the magnetic response. It is unclear whether dHvA oscillations exist in this region in the materials under study. We note that Terashima *et al.*[16] have recently observed quantum oscillations through B_{c2} and the peak effect region in YNi_2B_2C and observed a reduction in amplitude in this region possibly due to an increase in pinning.

The results obtained in the present work were collected in the region of weak pinning (II). It is clearly important to establish whether pinning results in a reduction of the observed dHvA signal in our measurements. As discussed in Sec. IV A 1, the characteristic shape of the hysteresis loops in Fig. 5, allows the estimation of $B^\star$. Since data was not collected in the peak effect region (I), the loop collected at 4.25 T corresponds to the worst case. We estimate $B^\star = 0.12$ mT. The dHvA data presented later were collected with $b = 50$ mT; if $b \gg B^\star$ then $B^\star$ is the variation of B over the sample. Phase smearing due a inhomogeneous magnetic field whose distribution has a half width δB lead to a damping factor $R_\phi = \exp(-2\pi F \delta B/B_0)$. Using values for $NbSe_2$, $F = 144$ T, $B_0 = 4.25$ T, and assuming $\delta B = B^\star$, gives $R_\phi = 0.97$, an order magnitude less than the observed attenuation. We conclude that flux pinning effects cannot explain the amplitude reduction in dHvA amplitude observed in the mixed state.

V. EXPERIMENTAL RESULTS

A. Determination of dHvA amplitude

It is essential to have a reliable method of determining the amplitude of the oscillations as a function of magnetic field with an estimate of the error for each point. To achieve this we have chosen to fit a general form of the LK expression to the data using the nonlinear Levenberg-Marquardt method.[58] We also include higher-order harmonics and impose a quadratic polynomial function for the background magnetization. The fitting function is given by

$$f(B_0, a_r, b_r, c_r, \alpha, \beta, \gamma) = \sum_{r=1}^{2} a_r \exp\left[r b_r \left(\frac{1}{B_0} - \frac{1}{B_i} \right) \right] \times \sin\left[2\pi r \left(\frac{F}{B_0} - \frac{1}{2} \right) + c_r \right] + \alpha + \beta B_0 + \gamma B_0^2. \quad (22)$$

The data are split up into equal intervals in $1/B_0$ of a length corresponding to $1\frac{1}{2}$ oscillations of the fundamental frequency and center $1/B_i$. In this way it is possible to extract the field-dependent amplitude $a_1(B_i)$ of the fundamental ($r = 1$) dHvA frequency. We choose not to impose any further constraints on the fitting procedure to ensure statistical independence between data points. After the set of points $\{a_1(B_i)\}$ have been corrected for the effect of field modulation,[59] they may be compared with [Eq. (2)]. We first use data with $B_i > B_{c2}$ to determine the normal state scattering rate τ_0^{-1} and then $R_s(B_i)$ is obtained by comparing the data collected at fields $B_i < B_{c2}$ with [Eq. (2)].

B. $NbSe_2$

The layered material $NbSe_2$ is a convenient material for studying the quantum oscillations in the vortex state. It has a modest T_c (≈ 7.2 K) and $B_{c2} = 12.7$ T for B_0 parallel to the layers (parallel to the a axis) and 4.2 T for B_0 perpendicular to the layers (parallel to the c axis). This implies that for orientations of the magnetic field away from the a axis a reasonable range of normal-state data can be obtained in our experimental set up in one single magnetic field sweep. As we shall discuss below the inclusion of normal-state data is of paramount importance for the analysis of the damping mechanisms in the vortex state. As discussed above, although $NbSe_2$ is a layered material with strong anisotropic properties its Fermi surface is three dimensional.

Figure 7(a) shows the dHvA signal in $NbSe_2$ for the field aligned 68.6° from the c axis. The Fourier spectrum gives $F = 155$ T and the effective mass was determined from the temperature dependence of the dHvA amplitude as $m^\star = 0.61 \pm 0.01\ m_e$. From left to right three regimes can be observed in Fig. 7(a); normal state, peak-effect region, and vortex state. Figure 7(b) shows the field dependence of the amplitude of the first harmonic $a_1(B_0)$ determined by the procedure described in Sec. V A. Fitting the data for $B_0 > B_{c2}$ yields a normal-state damping $\hbar \tau_0^{-1} = 1.31 \pm 0.02$ meV [Fig. 7(c)]. This value was then used to determine $\{R_s(B_i)\}$ which are shown in Fig. 8.

1. Comparison with theory

We can now proceed to compare $R_s(B_0)$ with the different theoretical models given in Sec. III B. In most models the product of the mass and gap parameter appears directly as $m_b\Delta(0)$ in the $R_s(B_0)$ damping equations or indirectly as $\Gamma/\Delta(0)$ in the DT model. Therefore, as a first step we will obtain the product $m_b\Delta(0)$ by fitting each model to the measured $R_s(B_0)$ and allowing $m_b\Delta(0)$ to vary. Then, in the next step we will discuss the various methods for determining the band mass and calculate the resulting superconducting gap parameters.

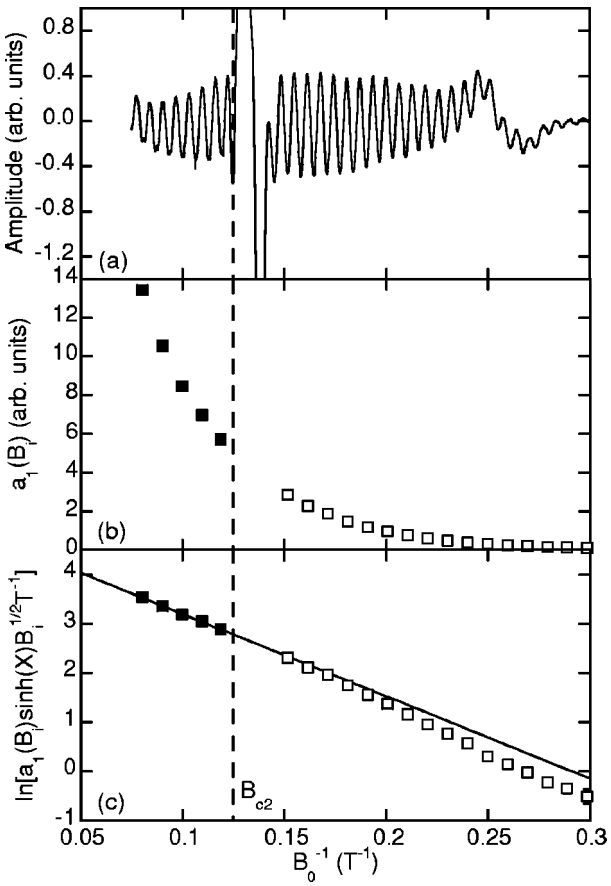

FIG. 7. (a) dHvA oscillations in $NbSe_2$ for $\theta = 68.6°$ between c axis and magnetic field, both above and below the critical field (which itself is dependent on the orientation in this anisotropic material). Trace was obtained by low frequency (5 Hz) field modulation method, at $T = 20$ mK. (b) Amplitude $a_1(B_i)$ calculated using the procedure described in Sec. V A and corrected for the effect of field modulation. (c) Field dependence of $\ln[a_i(B_i)\sinh(X)B_i^{1/2}T^{-1}]$ for the above data trace (sometimes referred to as Dingle plot) showing the onset of an additional attenuation on passing from the normal to the superconducting state at B_{c2}. The solid line is a fit to the data in the normal state.

Figure 8 shows a comparison of our measured $R_s(B_0)$ with four of the theoretical models. In each panel the solid line shows the result of fitting the model to the measured $R_s(B_0)$ and allowing $m_b\Delta(0)$ to vary. The fitted values of $m_b\Delta(0)$ are collected in Table I. The dashed line shows the results obtained using $\Delta(0) = 1.1$ meV, the literature value from infrared and Raman scattering experiments,[60,61] and $m_b = 0.52\ m_e$ (discussed below). From analyzing many different data traces we find that it is important to collect data in both the normal and superconducting states when comparing with the theoretical models. This provides an accurate estimate of τ_0^{-1} and constrains the amplitude in the vortex state.

In the last column of Table I the χ^2/ν values of the fits are listed which are representative of the quality of the fit. From these values and inspection of Fig. 8 we observe that the MSWS theory gives the best fit to the $NbSe_2$ data over a wide field range. The MMG theory can also provide the right functional form, however, with a lesser quality than the MSWS theory.

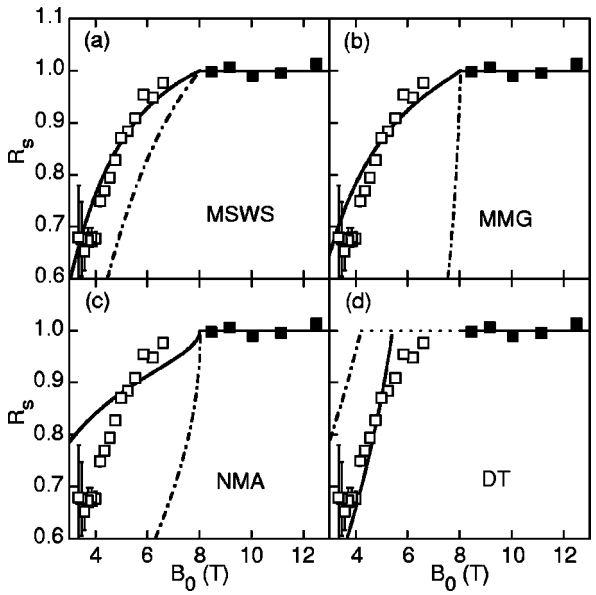

FIG. 8. $R_s(B_i)$ for $NbSe_2$ determined from the data shown in Fig. 7. Filled squares represent normal-state data and open squares vortex state data. The predictions of the theoretical models described in the text are shown by (i) dashed lines: model predictions calculated using the literature value of the superconducting gap and band mass and (ii) solid lines: model predictions fitted to the data allowing $m_b\Delta(0)$ to vary.

The third row in Table I gives results when using the NMA model [Eq. (18)] with the linear dependence on the gap parameter $[\propto n^{-1/4}\Delta'(0)]$. The temperature and energy scales of our experiment suggest that we are in the appropriate regime for the linear behavior to apply ($F_0 < 2\pi k_B T$), however, from the χ^2/ν value in Table I and Fig. 8 it is clear that the fit is very poor.

When we use the quadratic dependence on the gap parameter $[\propto n^{-1/2}\Delta'^2(0)]$ better quality fits can be obtained. For all our data the quadratic equation generates better fits than the linear equation which appears to contradict with the conditions explained in Sec. III B 5 and Ref. 53, which states that the linear equation should apply at low temperatures (<1 K for $NbSe_2$) and the quadratic equation for higher temperatures.

The limits of the DT model are more complex [see Eq. (16)] and the model involves one extra unknown parameter, the constant C in Eq. (13). This implies that this model cannot be fitted over the entire range for which we have obtained data in the vortex state, which is partly responsible for the larger value of χ^2/ν. In particular the region close to

TABLE I. Results of fitting $m_b\Delta(0)$ using the different theoretical models to the experimental data for $NbSe_2$ with the magnetic field titled by 68.6° from the c-axis. The column labeled χ^2/ν measures the quality of the fit.

Model	$m_b\Delta(0)$ ($m_e$meV)	χ^2/ν
MSWS [Eq. (10)]	0.36 ± 0.01	1.04
MMG [Eq. (12)]	0.06 ± 0.01	1.62
NMA [Eq. (18)]	0.09 ± 0.02	4.19
DT [Eq. (16)]	0.80 ± 0.02	2.49

TABLE II. Measured effective mass and calculated band mass obtained from the band structure calculation for $NbSe_2$. The last column lists the mass-enhancement factor which is given by $m^\star/m_b = 1+\lambda$.

	$m^\star$ (m_e)	m_b (m_e)	λ
Corcoran (Ref. 3)	0.61 ± 0.01	0.52	0.17

B_{c2}, when $\Delta(B_0) < \hbar\tau_0^{-1}$, is not included. In our data analysis the extra parameter C was kept fixed.

2. Band mass in $NbSe_2$

The cyclotron mass measured from the temperature dependence of the dHvA amplitude yields an effective mass which includes the effects of electron-electron and electron-phonon interactions. However, the *unrenormalized or band mass* appears to enter into the theoretical models described in Sec. III B. A knowledge of the correct band mass is one of the major uncertainties in our comparison between theory and experiment.

Corcoran *et al.*[3] have performed a self-consistent band structure calculation for $NbSe_2$ in the normal nonCDW state using a full potential linearized augmented plane wave (FLAPW) method. From this calculation a band mass[62] of $m_b = 0.52\ m_e$ was obtained when the magnetic field is aligned at 70° from the c axis, indicating a mass enhancement factor ($m^\star/m_b = 1+\lambda$), $\lambda = 0.17$ (See Table II). In the case of V_3Si, no detailed Fermi surface calculations are available, we therefore compared the calculated density of states with the measured specific heat coefficient. Applying this method to $NbSe_2$, with $\gamma_{exp} = 18.5$ mJ mol^{-1} K^{-2} (Ref. 63) and $\gamma_{calc} = 6.7$ mJ mol^{-1} K^{-2} (Ref. 3), suggests an overall mass-enhancement factor $\lambda = 1.77$.

3. Superconducting gap parameter in $NbSe_2$

With the above value of m_b and the fitted values of $m_b\Delta(0)$ for the different theoretical models listed in Table I we can obtain the superconducting gap parameter in each case which are listed in Table III. In the second row of Table III we have included the superconducting gap parameters when the measured effective mass is used. We note that these values are consistent with the values published in earlier work.[3] The formation of the low-temperature charge-density wave is not included in the band structure calculations and likely to alter m_b. As a result the values of $\Delta(0)$ would change proportionally for each model.

From Table III we observe that the MMG model grossly overestimates the attenuation of the oscillations in the mixed state. Similarly the NMA model results in a value of $\Delta(0)$ which fall well short of the literature value. The DT and MSWS models result in values of $\Delta(0)$ which are closest to the literature value of 1.1 meV.

4. Orientation dependence study

A common feature of all of the theoretical models described above is that the attenuation of the dHvA oscillations in the mixed state is a function of the superconducting gap $\Delta(0)$. Measurements performed as a function of orientation (θ) can then in principle yield the orientation dependence of the orbitally averaged superconducting gap. We note that the determination of the gap in this way is model dependent: in order to be specific we use the MSWS model which provides the best description of our $NbSe_2$ data. In order to determine the orientation dependence of the gap we need to know the θ dependence of τ_0^{-1} and m_b. Unfortunately, due to the large anisotropy of $B_{c2}(\theta)$ we are unable to collect data in the normal state for all orientations. The Fermi surface of $NbSe_2$ is an oblate ellipsoid[3] with $k_c = 0.05$ Å and $k_a = 0.338$ Å. Figure 9 summarizes our results for $NbSe_2$. The upper panel of Fig. 9 shows the mean free path $\ell_{mfp}(\theta)[=\nu_F\tau_0(\theta)]$. The solid line is a fit assuming the mean free path has the same symmetry as the Fermi surface expressed by $\ell_{mfp}(\theta) = \ell_{mfp}(0)/[1+\epsilon\cos^2(\theta)]$ which is used in our computation of $\Delta(0)$. The middle panel of Fig. 9 shows $m^\star(\theta)$, the solid line is a fit assuming $m^\star$ is proportional to the Fermi surface cross sectional area. We further assume that the renormalization parameter relating $m^\star$ and m_b, $\lambda(\theta) = 0.17$. Fitting the MSWS model for each orientation to the measured $R_s(B)$ then yields the gap variation in the lower panel of Fig. 9. The large errors in the final points are due to the uncertainties in the normal state scattering rate, band mass and Fermi velocity. Our results are not inconsistent with a constant gap, however there may be an increase in $\Delta(0)$ for larger θ.

Recently, Sanchez *et al.*[64] have performed specific heat measurements on $NbSe_2$ in high magnetic fields (up to 12 T) and found that their results could only be explained by assuming an anisotropic gap parameter given by

$$\Delta_\theta(0) = \Delta_0(0)(1+\epsilon_2\cos^2\theta). \tag{23}$$

θ is the angle between the wave vector and the c axis, $\Delta_0(0) = 1.6$ meV and $\epsilon_2 = -0.6$. In order to compare this gap with our dHvA results, we have to calculate the orbital average of $\Delta_\theta(0)$ with respect to our extremal Fermi surface orbit, which can be defined as[28]

TABLE III. Superconducting gap parameters for $NbSe_2$ obtained from $m_b\Delta(0)$ for the different theoretical models in Table I and m_b in Table II. The last row lists the values for $\Delta(0)$ when the experimentally measured *effective* mass is used.

		$\Delta(0)$ (meV)				
	m_b (m_e)	MSWS	MMG	NMA	DT	BCS
Corcoran	0.52	0.69 ± 0.02	0.12 ± 0.02	0.17 ± 0.04	1.50 ± 0.04	1.1
measured $m^\star$	0.61	0.59 ± 0.05	0.10 ± 0.03	0.14 ± 0.03	1.32 ± 0.03	1.1

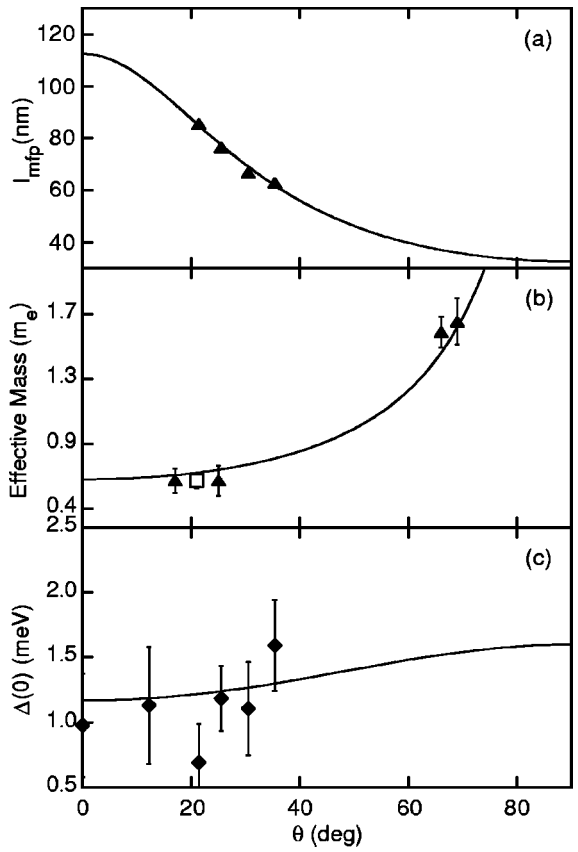

FIG. 9. (a) ℓ_{mfp} as a function of orientation. θ is the angle between the magnetic field and the a axis. The solid line is a fit assuming a simple anisotropic form for the impurity scattering (see text). (b) The measured effective mass versus θ. The open square is the result obtained in this work, the filled triangles are taken from Ref. 5. The solid line is a fit assuming $m^* \propto F$. (c) Orientation dependence of the energy gap $\Delta(0)$ derived from the MSWS model [Eq. (10)]. The solid line is the result from Eq. (24).

$$\sqrt{\langle \Delta_\theta^2(0) \rangle} = \frac{\oint \Delta_\theta^2(0) dt}{\oint dt} = \frac{\oint \Delta_\theta^2(0)/v_F dk}{\oint 1/v_F dk}, \qquad (24)$$

which is shown as the solid line in Fig. 9(c). Note that we have used Δ^2 in this calculation as this is the quantity which enters in Eq. (10). From the comparison of our values of $\Delta(0)$ with those calculated from the result by Sanchez *et al.*[64] it is difficult to discriminate between either an anisotropic or constant gap over the Fermi surface. The recent increases in the upper field attainable using superconducting magnets will allow more discriminating results to be obtained in future.

C. V_3Si

The experiments on V_3Si were performed using the same single crystal used in the pulsed field experiments of Corcoran *et al.*[8] Details can be found there. A series of dHvA oscillations for the magnetic field parallel to [001] and T $=20$ mK are shown in Fig. 10, together with the Fourier transform of the signal which gives a dominant frequency component at $F=1560\pm5$ T corresponding to approximately 10% of the Brillouin zone. Examination of the signal indicates that a small beating envelope is present, which is supported by the spectral analysis giving two low amplitude peaks at 1300 and 1410 T. The renormalized quasiparticle masses of these orbits were determined as $1.52\pm0.03\ m_e$ for $F=1560$ T, $1.3\pm0.3\ m_e$ for $F=1300$ T, and $1.7\pm0.4\ m_e$ for $F=1410$ T. In this work we will concentrate on the main frequency in the dHvA signal, although the two minor frequencies were included in the fitting of the dHvA signal to determine the amplitude of the main frequency. The calculated amplitude points $\{a_1(B_i)\}$ corrected for field modulation are shown in panel (c) of Fig. 10.

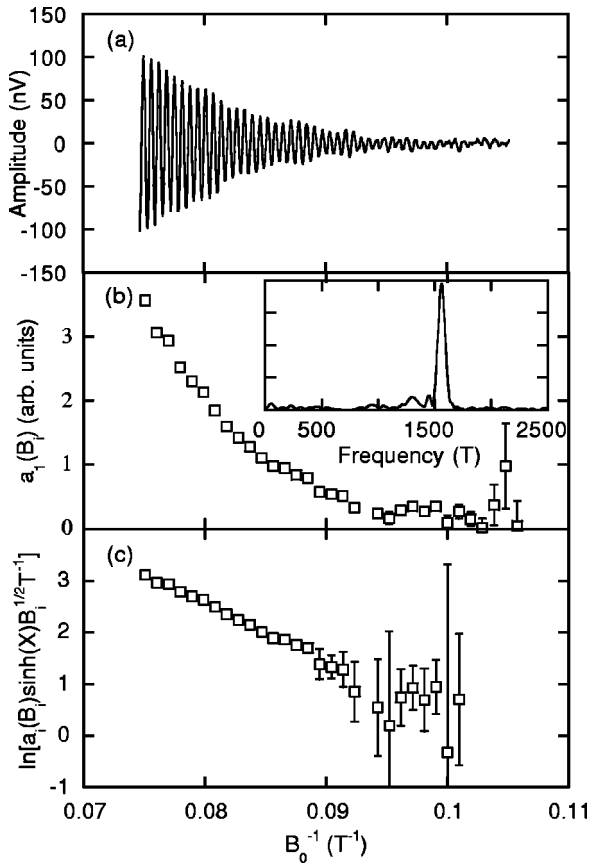

FIG. 10. (a) dHvA oscillations in V_3Si at 20 mK with the magnetic field parallel to [001]. (b) Amplitude $a_1(B_i)$ calculated using the procedure described in Sec. V A and corrected for the effect of field modulation. (c) Amplitude plot similar to Fig. 7.

The maximum field in our field modulation experiment is 13.5 T which is considerably below B_{c2} of 18.5 T for V_3Si. Therefore, we cannot apply the method used for $NbSe_2$ (Sec. V B) to compile the $R_s(B_0)$ values in the vortex state. Instead, we have analyzed data from a separate pulsed field experiment (up to 25 T) on the same crystal, yielding a normal-state damping $\hbar\tau_0^{-1}=1.22$ meV. In addition, we have allowed for the different sensitivities in both experiments by matching the amplitude of the modulation field data to the pulsed field data at 13.5 T. The resulting $R_s(B_0)$ values are plotted in Fig. 11 together with the $R_s(B_0)$ values from the pulsed field experiment. For the pulsed field data we have checked that the amplitude of the dHvA oscillations was not effected by heating as a result of the large dB/dt generated in such experiments. However, the sensitivity in

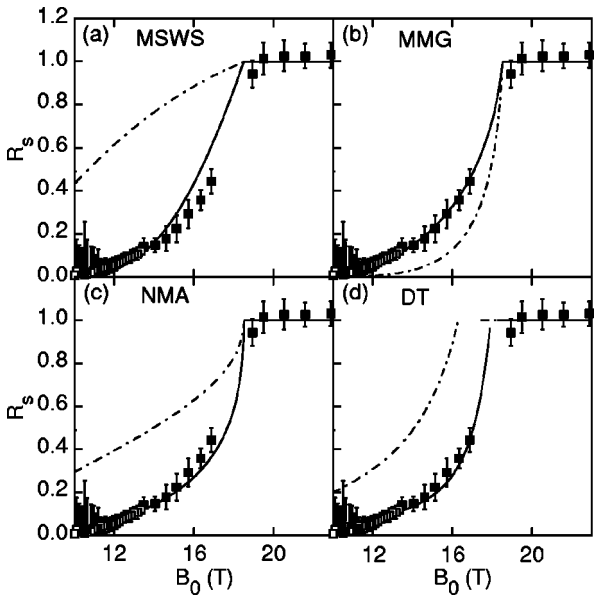

FIG. 11. Experimentally determined values of $R_s(B_0)$ for V_3Si for $\mathbf{B}||(001)$. In each panel the lines are the predictions of the theoretical models described in text. Dashed lines: model predictions calculated using the literature value of the superconducting gap and band mass. Solid lines: model predictions fitted to the data allowing $m_b\Delta(0)$ to vary.

modulation field experiments is much larger than in pulsed field experiments resulting in larger errors for the $R_s(B_0)$ values derived from the latter.

1. Comparison with theory

As for $NbSe_2$ we can compare $R_s(B_0)$ with the different theoretical models given in Sec. III B. Figure 11 shows the comparison of $R_s(B_0)$ with the four theoretical models. Again in each panel the dashed lines show the predictions of the models using $\Delta(0)=2.6$ meV, the literature value[65] for the superconducting gap and $m_b=0.9\ m_e$ (discussed below). The solid lines are the result of fitting each model to $R_s(B_0)$ and allowing $m_b\Delta(0)$ to float. The results are shown in Table IV.

In contrast to the result for $NbSe_2$, the MSWS theory applied to V_3Si gives a rather poor fit. In particular, the model does not fit the pulsed field data points (shown as filled squares in Fig. 11) above 13.5 T, although the fit through the data points obtained in the modulation field experiment (shown as open squares) is much better. This could be caused by errors in matching the data of two separate experiments, however, the other theoretical models do not appear to support this. The MMG theory provides the best quality fit for V_3Si over the entire field range. The NMA theory gives a reasonable fit. Finally, in the DT model we have again kept the constant C in Eq. (13) fixed. In contrast to $NbSe_2$, $\Delta(B_0)$ is much larger for V_3Si allowing, in this case, the DT model to be fitted to the entire range for which we have obtained data in the vortex state, resulting in a fairly good fit.

TABLE IV. Results of fitting $m_b\Delta(0)$ using the different theoretical models for the 1560 T orbit in V_3Si.

Model	$m_b\Delta(0)$ ($m_e$meV)	χ^2/ν
MSWS [Eq. (10)]	6.16 ± 0.23	5.7
MMG [Eq. (12)]	1.40 ± 0.06	1.1
NMA [Eq. (18)]	6.60 ± 0.35	1.3
DT [Eq. (16)]	4.05 ± 0.12	1.2

2. Band mass in V_3Si

In the case of V_3Si no direct calculations of the band mass for specific Fermi surface orbits are available. However, a number of calculations of the density of states have been reported[66–68] from which we can compute the linear specific heat coefficient. Comparing these with the measured linear specific heat coefficient[66] results in the total mass enhancement factor λ which we use to obtain the band mass from the measured effective mass. Table V lists the different parameters and band masses, which are in good agreement with each other.

3. Superconducting gap parameter in V_3Si

The calculation of Mattheiss[68] is the most recent and extensive of the calculations listed in Table III and we have chosen to use this band mass for our determination of the superconducting gap parameter. In Table VI the superconducting gap parameters are listed for the different theoretical models. Again we have included the superconducting gap parameters calculated using the measured effective mass which are in agreement with previously published[8,42] values.

From Table VI we observe that the MMG model again overestimates the damping of the oscillations in the vortex state. The MSWS and NMA model result in values for $\Delta(0)$ which are approximately twice as large as the literature value of 2.6 meV. For V_3Si the DT model gives a value of $\Delta(0)$ which is closest to the literature value. We note that most models appear to overestimate the value of $\Delta(0)$.

VI. DISCUSSION

The de Haas-van Alphen effect has now been observed in the superconducting state of many different materials. We

TABLE V. Calculated and measured (Ref. 66) linear specific heat coefficients (in mJ mol^{-1} K^{-2}) for V_3Si used to determine the unrenormalized band mass via $m_b=m^\star\gamma_{calc}/\gamma_{exp}$. The last column lists the mass-enhancement factor.

	γ_{calc}	γ_{exp}	$m^\star$ (m_e)	m_b (m_e)	λ
Jarlborg (Ref. 66)	37.6	55 ± 5	1.52 ± 0.03	1.0 ± 0.1	0.52
Klein (Ref. 67)	43.2	55 ± 5	1.52 ± 0.03	1.2 ± 0.1	0.26
Mattheiss (Ref. 68)	34.5	55 ± 5	1.52 ± 0.03	0.9 ± 0.1	0.69

TABLE VI. Superconducting gap parameters for V_3Si obtained from $m_b\Delta(0)$ for the different theoretical models in Table IV and m_b in Table V. The last row lists the values for $\Delta(0)$ when the experimentally measured *effective* mass is used.

		$\Delta(0)$ (meV)				
	m_b (m_e)	MSWS	MMG	NMA	DT	BCS
Mattheiss	0.9	6.80 ± 0.80	1.60 ± 0.27	7.30 ± 0.90	4.50 ± 0.50	2.6
measured $m^\star$	1.52	4.10 ± 0.15	0.92 ± 0.04	4.32 ± 0.23	2.53 ± 0.08	2.6

have compared a number of theoretical models with our experimental observations. Perhaps the simplest theory is that of Miyake which assumes an extremely high GL parameter $\kappa\gg1$ and thus a constant gap in the space between the vortices. In both materials studied, this model grossly overestimates the attenuation of the dHvA oscillations suggesting that the spatial variation of the order parameter, due to the Abrikosov vortex lattice, is responsible for the large amplitude of the observed dHvA oscillations. The MSWS and DT models which include the spatial variation of the order parameter provide a better description of our observations. We note that in these two models the attenuation is a function of the spatially averaged square of the order parameter. From the comparison of the fitting results for both materials studied, it is clear that the theory position needs to be clarified. None of the theories tested can consistently account for the damping of the dHvA oscillations in *both* compounds.

We note that the major uncertainty in a critical comparison of theory with the observed dHvA oscillations is our lack of knowledge of the bare or unrenormalized band mass. In spite of this, we have shown how the dHvA effect may, in a model-dependent manner, yield information about the superconducting state.

Dukan and Tešanović[42] argued that the dHvA effect is a result of the presence of a small portion of the Fermi surface containing a coherent normal band of quasiparticles, while the rest of it is gapped. In Table VII we have listed the mean free path for both materials. The vortex separation varies from $\sim$200 to $\sim$100 Å for fields between 5 and 20 T. Therefore, for the magnetic field range used in our experiments ℓ_{mfp} extends over many vortex lattice unit cells, ensuring that the electron motion is indeed coherent.

TABLE VII. Summary of the parameters used for $NbSe_2$ and V_3Si in the comparison of $R_s(B)$ with the theoretical models.

	$NbSe_2$	V_3Si	Origin
F (T)	153	1560	experimental
$m^\star$ (m_e)	0.61	1.52	experimental
λ	0.17	0.69	band structure theory
m_b (m_e)	0.52	0.9	calculated using λ
ν_F ($\times10^5$ ms^{-1})	1.75	2.80	calculated using m_b and F
$\hbar\tau_0^{-1}$ (meV)	1.31	1.22	experimental
$\Delta(0)$ (meV)	1.1	2.6	literature values
B_{c2} (T)	8.01	18.5	experimental
ℓ_{mfp} (Å)	841	1555	calculated using τ_0^{-1}
κ	14-54	17	literature values

Some of the models predict that $\hbar\tau_s^{-1}\propto\Delta^2(B)\Lambda$ or $\Delta^2(B)$. Figure 12 shows that our data for $NbSe_2$ does indeed obey this relation very well. On the basis of this the NMA model [Eq. (18)] must be rejected. In the case of V_3Si the agreement is not so good. As discussed before there can be several experimental explanations for this. One effect not considered by most theories is the impurity scattering rate in the vortex state. All but the theory of Dukan and Tešanović assume τ_0^{-1} is constant as a function of magnetic field. Dukan and Tešanović explicitly treat this problem and find that τ_0^{-1} has to be calculated self-consistently resulting in a magnetic-field-dependent $\tau^{-1}(B)$ given in Eq. (14). From this equation we observe that the effect of $\tau^{-1}(B)$ for $NbSe_2$ is small because $\Delta(B)$ is small, however, for V_3Si with a much larger gap the effect is sizable, as was shown explicitly in Ref. 42.

VII. SUMMARY

A quantitative study and analysis of the dHvA effect in the vortex state of $NbSe_2$ and V_3Si has been presented. We have shown that, for these materials, the additional attenuation of the oscillations cannot be explained in terms of the macroscopic field variation, or pinning, of the flux line lattice. Thus the additional attenuation has a microscopic ori-

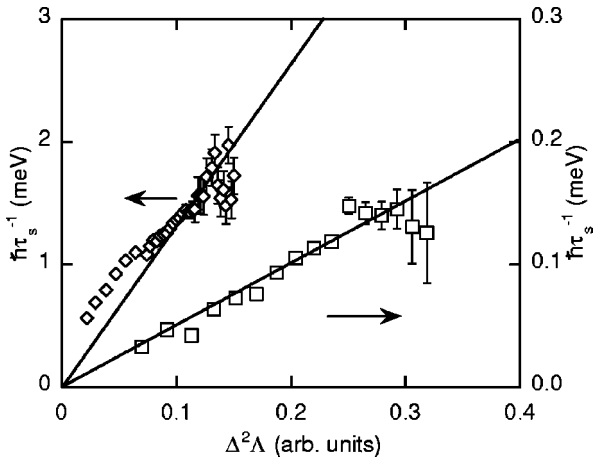

FIG. 12. $\hbar\tau_s^{-1}$ as a function of $\Delta^2(B)\Lambda$. $\Delta(0)$ has been set to unity. The open diamonds refer to V_3Si and the open squares to $NbSe_2$ and the lines are linear fits in each case.

gin. The macroscopic field variation and pinning could be of importance under different experimental circumstances or in different materials. We have compared various theoretical models with our experimental observations and shown that models which incorporate the spatial variation of the order parameter give the best results. However, none of these models consistently explain the data in both materials studied indicating that more theoretical work is required.

ACKNOWLEDGMENTS

The authors warmly acknowledge discussions with M. N. Cuthbert, M. Norman, B. L. Györffy, Z. Tešanović, and R. Corcoran, which have clarified these issues. The financial support of the Engineering and Physical Sciences Research Council and the Royal Society is gratefully acknowledged. One of the authors (T.J.B.M.J.) would like to acknowledge financial support from the Leverhulme Trust.

[1] J. E. Graebner and M. Robbins, Phys. Rev. Lett. **36**, 422 (1976).
[2] Y. Onuki, I. Umehara, T. Ebihara, N. Nagai, and T. Takita, J. Phys. Soc. Jpn. **61**, 692 (1992).
[3] R. Corcoran, P. Meeson, Y. Onuki, P. A. Probst, M. Springford, K. Takita, H. Harima, G. Y. Guo, and B. L. Györffy, J. Phys.: Condens. Matter **6**, 4479 (1994).
[4] R. Corcoran, N. Harrison, C. J. Haworth, S. M. Hayden, P. Meeson, M. Springford, and P. J. van der Wel, Physica B **206-207**, 534 (1995).
[5] E. Steep, S. Rettenberger, A. G. M. Janssen, W. Joss, W. Bilberacher, E. Bucher, and C. S. Oglesby, Physica B **206-207**, 162 (1995).
[6] S. Rettenberger, E. Steep, F. Meyer, A. G. M. Janssen, W. Joss, P. Wyder, W. Biberacher, E. Bucher, and C. S. Oglesby, Physica B **21**, 244 (1995).
[7] F. Mueller, D. H. Lowndes, Y. K. Chang, A. J. Arko, and R. S. List, Phys. Rev. Lett. **68**, 3928 (1992).
[8] R. Corcoran, N. Harrison, S. M. Hayden, P. Meeson, M. Springford, and P. J. van der Wel, Phys. Rev. Lett. **72**, 701 (1994).
[9] N. Harrison, S. M. Hayden, P. Meeson, M. Springford, P. J. van der Wel, and A. A. Menovsky, Phys. Rev. B **50**, 4208 (1994).
[10] R. G. Goodrich, C. Grienier, D. Hall, A. Lacerda, E. G. Haanappel, D. Rickel, T. Northington, R. Schwarz, F. M. Mueller, D. D. Koeling, J. Vuillemin, L. van Bockstal, M. L. Norton, and D. H. Lowndes, J. Phys. Chem. Solids **54**, 1251 (1993).
[11] M. Hedo, Y. Inada, T. Ishida, E. Yamamoto, Y. Haga, Y. Onuki, M. Higuchi, and A. Hasegawa, J. Phys. Soc. Jpn. **64**, 4535 (1995).
[12] Y. Inada, M. Hedo, T. Ishida, E. Yamamoto, Y. Haga, and Y. Onuki, Physica B **230-232**, 387 (1997).
[13] M. Heinecke and K. Winzer, Z. Phys. B **98**, 147 (1995).
[14] T. Terashima, H. Takeya, S. Uji, K. Kadowaki, and H. Aoki, Solid State Commun. **96**, 459 (1995).
[15] G. Goll, M. Heinecke, A. G. M. Jansen, W. Joss, L. Nguyen, E. Steep, K. Winzer, and P. Wyder, Phys. Rev. B **53**, R8871 (1996).
[16] T. Terashima, C. J. Haworth, H. Takeya, S. Uji, and H. Aoki, Phys. Rev. B **56**, 5120 (1997).
[17] H. Ohkuni, T. Ishida, Y. Inada, Y. Haga, E. Yamamoto, Y. Onuki, and S. Takahashi, J. Phys. Soc. Jpn. **66**, 945 (1997).
[18] C. Bergemann, S. R. Julian, G. J. McMullan, B. K. Howard, G. G. Lonzarich, P. Lelay, J. P. Brison, and J. Flouquet, Physica B **230-232**, 348 (1997).
[19] P. J. van der Wel, J. Caulfield, R. Corcoran, P. Day, S. M. Hayden, W. Hayes, M. Kurmoo, P. Meeson, J. Singleton, and M. Springford, Physica C **235-240**, 2453 (1994).
[20] C. M. Fowler, B. L. Freeman, W. L. Hults, J. C. King, F. M. Mueller, and J. L. Smith, Phys. Rev. Lett. **68**, 534 (1992).
[21] G. Kido, K. Komorita, H. Katayama-Yoshida, and T. Takahashi, J. Phys. Chem. Solids **52**, 1465 (1991).
[22] G. Kido, H. Katayama-Yoshida, and T. Takahashi, Jpn. J. Appl. Phys., Part 1 **7**, 247 (1992).
[23] M. Springford, N. Harrison, P. Meeson, and P. A. Probst, Phys. Rev. Lett. **69**, 2453 (1992).
[24] E. G. Haanappel, W. Joss, I. D. Wagner, P. Wyder, K. Trubenbach, H. Mattausch, A. Simon, F. M. Mueller, and S. Ashkenazy, Physica C **209**, 39 (1993).
[25] E. G. Haanappel, W. Joss, P. Wyder, S. Ashkenazy, F. M. Mueller, K. Trubenbach, H. Mattausch, S. Simon, and M. Osofsky, J. Phys. Chem. Solids **54**, 1261 (1993).
[26] A. I. Bykov, M. I. Dolotenko, N. P. Kolokolchikov, Yu. B. Kudasov, V. V. Platonov, O. M. Tatsenko, A. I. Golovashkin, O. M. Ivanenko, and K. V. Mitsen, Physica B **211**, 241 (1995).
[27] D. Shoenberg, *Magnetic Oscillations in Metals*, Cambridge Monograph on Physics (Cambridge University Press, Cambridge, 1984).
[28] A. Wasserman and M. Springford, Adv. Phys. **45**, 471 (1996).
[29] R. E. Prange and A. Sachs, Phys. Rev. **158**, 672 (1967).
[30] S. Engelsberg and G. Simpson, Phys. Rev. B **2**, 1657 (1970).
[31] J. W. Wilkins, in *Electrons at the Fermi Surface*, edited by M. Springford (Cambridge University Press, Cambridge, 1980).
[32] P. C. Hohenberg and W. Kohn, Phys. Rev. **136**, B864 (1964).
[33] W. Kohn and L. J. Sham, Phys. Rev. **140**, A1133 (1965).
[34] J. M. Delrieu, J. Low Temp. Phys. **6**, 197 (1972).
[35] E. H. Brandt, Rep. Prog. Phys. **58**, 1465 (1995), and references therein.
[36] K. Maki and T. Tsuzuki, Phys. Rev. **139**, A868 (1965).
[37] E. H. Brandt, J. Low Temp. Phys. **73**, 355 (1988).
[38] T. Maniv, R. S. Markiewicz, I. D. Vagner, and P. Wyder, Physica C **153-155**, 1179 (1988).
[39] T. Maniv, A. I. Rom, I. D. Vagner, and P. Wyder, Phys. Rev. B **46**, 8360 (1992).
[40] T. Maniv, A. I. Rom, I. D. Vagner, and P. Wyder, Physica C **235**, 1541 (1994).
[41] T. Maniv, A. I. Rom, I. D. Vagner, and P. Wyder, Solid State Commun. **101**, 621 (1997).
[42] S. Dukan and Z. Tešanović, Phys. Rev. Lett. **74**, 2311 (1995).
[43] A. Wasserman and M. Springford, Physica C **194-196**, 1801 (1994).
[44] K. Maki, Phys. Rev. B **44**, 2861 (1991).
[45] U. Brandt, W. Pesch, and L. Tweordt, Z. Phys. **201**, 209 (1967).
[46] M. J. Stephen, Phys. Rev. B **43**, 1212 (1991).
[47] M. J. Stephen, Phys. Rev. B **45**, 5481 (1992).
[48] K. Miyake, Physica B **186-188**, 115 (1993).
[49] P. Miller and B. L. Györffy, J. Phys.: Condens. Matter **7**, 5579 (1995).

[50] S. Dukan and Z. Tešanović, Phys. Rev. B **49**, 13 017 (1994).
[51] M. R. Norman, A. H. MacDonald, and H. Akera, Phys. Rev. B **51**, 5927 (1995).
[52] M. R. Norman and A. H. MacDonald, Phys. Rev. B **54**, 4239 (1996).
[53] M. R. Norman (private communication).
[54] A. M. Campbell and J. E. Evetts, Adv. Phys. **21**, 199 (1972).
[55] C. P. Bean, Rev. Mod. Phys. **36**, 31 (1964).
[56] A. B. Pippard, Philos. Mag. **19**, 217 (1968).
[57] A. L. Larkin and Y. N. Ovchinnikov, J. Low Temp. Phys. **34**, 409 (1978).
[58] P. R. Bevington, *Data Reduction and Error Analysis for the Physical Sciences* (McGraw-Hill, New York, 1969).
[59] A. V. Gold, in *Solid State Physics: Electrons in Metals*, edited by J. F. Cochran and R. R. Hearing (Gordon and Breach, New York, 1968).
[60] B. P. Clayton and R. F. Frindt, Solid State Commun. **18**, 1881 (1971).
[61] D. H. Lee, L. W. Dubeck, and F. Rothwarf, Phys. Lett. **53A**, 379 (1975).
[62] In Ref. 8 a band mass of $0.46m_e$ was used to calculate the mass enhancement factor. However, in this calculation the measured and calculated dHvA frequencies did not agree. In order to obtain this agreement the Fermi energy was shifted by 7 mRyd, resulting in a band mass of $m_b = 0.52\ m_e$.
[63] P. Garoche, J. J. Veyssie, P. Manuel, and P. Molinie, Solid State Commun. **19**, 455 (1976).
[64] D. Sanchez, A. Junod, J. Muller, H. Berger, and F. Levy, Physica B **204**, 167 (1995).
[65] R. Hackle, R. Kaiser, and S. Schicktanz, J. Phys. C **16**, 1729 (1983).
[66] A. Junod, T. Jarlborg, and J. Muller, Phys. Rev. B **27**, 1568 (1983).
[67] B. M. Klein, L. L. Boyer, and D. A. Papaconstantopoulos, Phys. Rev. Lett. **42**, 530 (1979).
[68] L. F. Mattheiss and W. Weber, Phys. Rev. B **25**, 2248 (1982).